Geophysical Research Letters

RESEARCH LETTER
10.1029/2024GL111059

Global Distribution and Seasonality of Martian Atmospheric HCl Explained Through Heterogeneous Chemistry

Paul M. Streeter[1], Kylash Rajendran[1], Stephen R. Lewis[1], Kevin S. Olsen[2], Alexander Trokhimovskiy[3], Oleg Korablev[3], and Manish R. Patel[1,4]

[1]School of Physical Sciences, The Open University, Milton Keynes, UK, [2]Department of Physics, University of Oxford, Oxford, UK, [3]Space Research Institute (IKI), Moscow, Russia, [4]Space Science and Technology Department, Science and Technology Facilities Council, Rutherford Appleton Laboratory, Oxfordshire, UK

Key Points:

- Latitudinal and seasonal behavior of observed Mars atmospheric hydrogen chloride (HCl) can be explained by heterogeneous chlorine chemistry
- Observed seasonal, hemispheric, and vertical HCl variation is qualitatively captured by heterogeneous dust emission and ice absorption
- We also predict enhanced north polar HCl during the aphelion season, not currently seen in Trace Gas Orbiter observations

Supporting Information:

Supporting Information may be found in the online version of this article.

Correspondence to:

P. M. Streeter,
paul.streeter@open.ac.uk

Citation:

Streeter, P. M., Rajendran, K., Lewis, S. R., Olsen, K. S., Trokhimovskiy, A., Korablev, O., & Patel, M. R. (2025). Global distribution and seasonality of Martian atmospheric HCl explained through heterogeneous chemistry. *Geophysical Research Letters*, *52*, e2024GL111059. https://doi.org/10.1029/2024GL111059

Received 26 JUN 2024
Accepted 20 JAN 2025

Abstract Recent observations from the ExoMars Trace Gas Orbiter (TGO) have revealed the presence of hydrogen chloride (HCl) in the martian atmosphere. HCl shows strong seasonality, primarily appearing during Mars' perihelion period before decreasing faster than projected from photolysis and gas-phase chemistry. HCl profiles also display local anti-correlation with water ice aerosol. One candidate explanation is heterogeneous chemistry. We present the first results from a heterogeneous chlorine chemistry scheme incorporated into a Mars global climate model (GCM), with atmospheric dust/water ice parameterized as an HCl source/sink respectively. Results were compared against a Mars GCM with gas-phase only chlorine chemistry and observations from TGO's Atmospheric Chemistry Suite. We found that the heterogeneous scheme significantly improved the modeled HCl seasonal, latitudinal, and vertical distribution, supporting a crucial role for heterogeneous chemistry in Mars' chlorine cycle. Remaining discrepancies show that further work is needed to characterize the exact aerosol reactions involved.

Plain Language Summary The ExoMars Trace Gas Orbiter (TGO) recently detected hydrogen chloride (HCl) for the first time in the martian atmosphere. Observations show that HCl appears around southern summer, when Mars is closest to the Sun, and abruptly decreases at the end of this season. This variation occurs on timescales far shorter than the expected photochemical lifespan of HCl, implying other processes are responsible. One possible explanation is heterogeneous chemistry: reactions between gaseous species and atmospheric dust and/or water ice. To investigate we implemented such a scheme into a Mars global climate model, whereby atmospheric dust and water ice aerosol act (respectively) as a source and sink for HCl. Comparing to TGO observations, we found that including heterogeneous chemistry significantly improved HCl representation. We were able to reproduce key observed features such as the HCl seasonal cycle, the greater HCl presence in the southern hemisphere, and to an extent the complex vertical structure. This strongly suggests that heterogeneous chemistry is a crucial component of the martian chlorine cycle. However, some questions remain, such as whether there is a causal relationship between dust storms and HCl presence. Further work is therefore needed to understand the relationships between aerosols and chlorine species.

1. Introduction

Atmospheric hydrogen chloride (HCl) has recently been detected from orbit in the martian atmosphere, first by the Atmospheric Chemistry Suite (ACS) (Korablev et al., 2021) and confirmed by Nadir and Occultation for MArs Discovery (NOMAD) (Aoki et al., 2021) spectrometers aboard the ExoMars Trace Gas Orbiter (TGO). Previous ground-based attempts to find chlorine species had only established upper detection limits (e.g., Hartogh et al., 2010; Villanueva et al., 2013), implying an absence of contemporary chlorine-based chemistry in Mars' atmosphere. TGO's HCl measurements of 1–4 ppbv therefore open up a new avenue of chemical activity in the Martian atmosphere to investigate.

The seasonal changes in TGO's orbital HCl measurements suggest an important relationship between HCl and atmospheric aerosol and water presence. In Mars Year (MY) 34, the measured HCl abundance increased during the Global Dust Storm (GDS) and decreased after its end (Korablev et al., 2021). In MY 35, HCl mixing ratios rapidly rose in both hemispheres with the advent of the perihelion (dusty) season from $L_s = 180°$, while remaining low in the clearer aphelion season, with values of 0.1–0.4 ppbv in both hemispheres (Olsen et al., 2021). This increase during the MY 35 perihelion season also demonstrated that the observed HCl increases are a seasonal phenomenon, not tied solely to GDS occurrences (Aoki et al., 2021).

In addition to this broad correlation with the dust seasonal loading, there appears to be a significant link between HCl and water (Aoki et al., 2021; Olsen et al., 2021). More recent analysis of MY 34–36 HCl profiles and comparison to Mars Climate Sounder (MCS) dust and water ice observations shows a relatively weak HCl-dust correlation, and a much stronger HCl-water vapor correlation (Olsen et al., 2024b). ACS profiles also show apparent "ice holes" where rapid reductions in HCl abundance align with water ice layers, suggesting a role for water ice as an HCl sink (Luginin et al., 2024). While retrieved HCl and water ice abundances show only a weak anti-correlation between the two, climatologies show that HCl and water ice do not generally both exist in measurable quantities at the same altitudes (Olsen et al., 2024a). This difference in residence heights of HCl and water ice (Olsen et al., 2024b) together with the "ice holes" implies a possible role for water ice clouds in explaining the observed HCl distribution, including the observed rapid drop-off in HCl (tens of sols) after the dusty season despite its projected photochemical lifespan of 90–1,000 sols below 15 km, depending on location (Aoki et al., 2021). This new potential role for water ice as a sink has never been tested in a global Mars model.

The results of observational analysis suggest that the sources of atmospheric HCl on Mars are likely associated with heterogeneous chemistry. On Earth, stronger acids than HCl, such as H_2SO_4 and HNO_3, can displace and push out HCl from chloride-containing aerosol particles such as sea salt (Simpson et al., 2015). Such reactions are rapid and so likely proceed near the surface of the particle (George & Abbatt, 2010). There is observational evidence of such reactions on the Martian surface. The Curiosity rover detected gaseous HCl during its heating of rock and soil samples (Clark et al., 2020), and its results indicate that the reaction of water with perchlorates and/or chlorides caused this HCl release. ACS measurements of stable HCl isotopologues ($H^{35}Cl$ and $H^{37}Cl$) found a ratio almost identical to that on Earth and consistent with the martian surface, implying that observed atmospheric HCl likely originates from dust and does not have a long enough lifetime to undergo noticeable fractionation (Trokhimovskiy et al., 2021). NOMAD-derived Cl isotopic ratios also show values compatible with the Martian surface, again suggesting limited fractionation and instead the dominance of HCl creation/sequestration (Liuzzi et al., 2021).

Recent 1D modeling, using measured aerosol profiles, of Martian HCl photochemistry suggests that gas-phase chemistry alone is unable to reproduce the orbitally observed HCl distribution, but that addition of heterogeneous processes can improve the observational match. Krasnopolsky (2022) included five possible heterogeneous chlorine reactions in a 1D model. These consisted of modeling dust as a heterogeneous source for atmospheric chlorine species, and dust and water ice as heterogeneous sinks. They found that the modeled lifespan and distribution of HCl at 5–35 km was consistent with observations, and abundances rose above 35 km where observations are sparser. They also found little effect on major photochemical products from HCl chemistry. Taysum et al. (2024) included UV photolysis of hydrated perchlorates in dust particles, and produced a HCl seasonal and temporal distribution consistent with observations, which included declining HCl abundances with altitude. However, the lack of atmospheric transport within 1D models necessarily curtails their ability to fully represent how the HCl distribution, such as in latitude, might be affected by global dynamics.

In this study we use a global climate model (GCM) for Mars with both gas-phase and heterogeneous chlorine chemistry to investigate the 3D impact of heterogeneous processes on the modeled HCl distribution. One key advantage of using a GCM over 1D modeling is in being able to examine the global, self-consistent behavior of HCl over multiple Mars years, both where HCl observations are present for comparison and validation, but also examine HCl behavior at times and locations where observations are lacking. By using a GCM, transport of HCl and relevant species/tracers such as water vapor, dust, and water ice are also explicitly included in our simulations. The aim is to investigate if heterogeneous chlorine chemistry can help explain the observed behavior of HCl in the Martian atmosphere, and pave the way for greater understanding of the chlorine cycle on Mars.

2. Methods

2.1. Model Overview

The GCM used in this study was the Mars Planetary Climate Model (Forget et al., 1999) and specifically the variant with a spectral dynamical core (Hoskins & Simmons, 1975) employed by the Open University. This martian GCM (henceforth, the MGCM) contains an extensive range of routines to represent the specific features of the martian atmosphere, including radiative transfer, atmospheric dust radiative effects and transport, water ice microphysics, the CO_2 cycle, and photochemistry. Dust transport is performed via a two-moment scheme where

dust mass mixing ratios and number densities are advected by the model, assuming a log normal dust size distribution, and opacities are scaled according to observed column dust opacities (Madeleine et al., 2011). The MGCM has an established heritage of use for investigating varied phemonena such as dust lifting and transport (Chapman et al., 2017; Mulholland et al., 2015; Newman et al., 2002), large-scale dynamics (S. R. Lewis & Read, 2003; S. R. Lewis et al., 2016; Rajendran et al., 2021), the water cycle and atmospheric escape (Holmes et al., 2021; Steele, Lewis, Patel, Montmessin, et al., 2014), polar processes (Streeter et al., 2021; Streeter, Lewis, et al., 2024), and atmospheric chemistry (Brown et al., 2022; Holmes et al., 2018). The water cycle in the MGCM is self-consistent but, unlike the dust cycle, not directly constrained by observations. While attempts have been made to directly assimilate observed water ice extinction profiles (Steele, Lewis, & Patel, 2014), the problem is a challenging one and for this work we have decided to focus on using a self-consistent water cycle that broadly agrees with the observed cycle.

2.2. Gas-Phase Chlorine Chemistry

For this study, the MGCM was run with the photochemical scheme described in Rajendran et al. (2025), but with the addition of heterogeneous chlorine reactions. As described in Rajendran et al. (2025), the photochemistry scheme of Lefèvre et al. (2004) was modified to add 11 new chlorine species: hydrogen chloride (HCl), atomic chlorine (Cl), molecular chlorine (Cl_2), chlorine monoxide (ClO), hydrogen hypochlorite (HOCl), chlorine peroxy (ClOO), chlorine dioxide (OClO), dichlorine dioxide (Cl_2O_2), chlorine trioxide (ClO_3), chlorine perchlorate (Cl_2O_4), and perchlorate acid ($HClO_4$). This updated chlorine scheme was based on the photochemistry scheme presented in Catling et al. (2010). Tables S1 and S2 in Supporting Information S1 contain the gas-phase and photolysis reactions included in the photochemical routine used for this study (values taken from Campbell and Gray (1973); Burkholder et al. (2019); Baulch et al. (2005); Simonaitis and Heicklen (1975); Zhu and Lin (2004); Xu and Lin (2003); Atkinson et al. (2007); Minschwaner et al. (1992); Yoshino et al. (1988); Brasseur and Solomon (1986); Parkinson et al. (2003); B. Lewis and Carver (1983); Yoshino, Esmond, Sun, et al. (1996); Sander et al. (2006); Cheng et al. (1999); Yoshino, Esmond, Parkinson, et al. (1996); Schergers and Welge (1968); Sander et al. (2003); Barnes et al. (1998); Trolier et al. (1990); Sander et al. (2011); Wahner et al. (1987); Papanastasiou et al. (2009)). Details of the (photo)chemical timestepping can be found in Rajendran et al. (2025). We differ by not including adsorption of perchloric acid ($HClO_4$) onto the martian surface. We decided against its inclusion for reasons of methodological clarity, as we wished to focus on specifically atmospheric HCl heterogeneous reactions. From sensitivity testing by Rajendran et al. (2025) it was calculated that the scheme removed atmospheric chlorine at a rate of approximately 0.001%–0.1% per Mars year (depending on surface uptake coefficient) which is miniscule compared to the variation we discuss below; we therefore feel confident that the inclusion of the scheme would have no significant effect on our analysis.

2.3. Heterogeneous Chlorine Chemistry

In addition to the gas-phase chlorine reactions described, we also implement heterogeneous reactions between HCl and Martian atmospheric dust and water ice. We follow the scheme described by Krasnopolsky (2022), adopting mineral dust as a heterogeneous source and water ice as a heterogeneous sink for atmospheric HCl. Specifically, we adopt the following two reactions (R1 and R4 respectively from Krasnopolsky (2022)):

$$XCl_k(s) + H(g) \rightarrow XCl_{k-1}(s) + HCl(g) \quad (1)$$

$$HCl(g) + H_2O_{ice}(s) \rightarrow \text{products}(s) \quad (2)$$

where X is a metal in chloride, with likely candidates for XCl_k being $FeCl_3$ and NaCl. The former is favored due its high energy yield δE (Krasnopolsky, 2022). Free atomic H is available from photolysis of water vapor (Krasnopolsky, 2022). The products from Equation 2 are nominally water ice with HCl adsorbed onto the surface and/or interior, but for the purposes of this study the HCl is effectively removed from the system and only the water ice remains.

For the reaction rate, Q, at altitude z, of a heterogeneous reaction we use

$$Q(\zeta) = \frac{1}{4}\,\gamma(\zeta)\; n_g(\zeta)\; V_t(\zeta)\; A(\zeta) \quad (3)$$

where $\zeta = (t, z, \phi, \psi)$ represents time, altitude, latitude, and longitude respectively, γ represents the reaction probability, n_g is the number density of the gas reactant, V_t is the thermal velocity of the gas reactant, and A is the aerosol surface area per unit volume of air. It should be noted that our heterogeneous parametrization does not take into account the possible effects of diffusion-limited uptake (Jacob, 2000), whereby the molecular diffusion rate of H on dust particles and/or HCl on water ice particles may serve as a bottleneck on further uptake.

Here, γ is a parameter incorporating the probability of the reaction occurring, including the share of reactants in the aerosol. Due to its poorly constrained nature, for this study γ was empirically tuned to a value of 0.01 for dust heterogeneous reactions and 0.1 for water ice heterogeneous reactions. This tuning was conducted by exploring the parameter space of the γ value for both dust and ice. A higher value of γ for dust results in greater HCl production, and for ice results in greater HCl adsorption. The best fit for these γ values was obtained by comparing the resultant HCl magnitudes and distribution to retrieved HCl, with all else held equal. In particular, γ values for dust above 0.01 resulted in dramatically overestimated HCl magnitudes.

The thermal velocity, V_t, is defined

$$V_t(\zeta) = \sqrt{\frac{8\ k_B\ T(\zeta)}{\pi\ m(\zeta)}} \tag{4}$$

where k_B is the Boltzmann constant, T is the atmospheric temperature, and m is the molecular mass of HCl. The aerosol surface area per unit volume of air, A, is calculated according to

$$A(\boldsymbol{\zeta}) = 4\ \pi\ f_a\ N_a(\zeta)\ r_a(\zeta)^2\ \rho(\zeta) \tag{5}$$

where the subscript a represents the aerosol kind (dust or water ice), f_a is a constant multiplying factor for the mass-mean radius based on the variance of the log normal particle size ($f_d = 1.23$ and $f_i = 2$), N_a is the number density of the aerosol kind (scaled to match observed column opacities), r_a is the geometric mean radius of the aerosol kind, and ρ is the atmospheric density. Refer to Figure S5 in Supporting Information S1 for information on approximate particle size ranges in the MGCM. The dust number density N_d is taken directly from the MGCM, which contains N_d as a freely transported prognostic field as part of the two-moment dust transport scheme (Madeleine et al., 2011). Water ice, however, is not represented with a two moment scheme. For the water ice number density N_i, therefore, we use the number density of cloud condensation nuclei (CCN) in the MGCM's water ice cloud microphysics scheme. This is a two-moment scheme separate to the dust two-moment scheme, including only the "activated" dust population where cloud nucleation is judged to occur, and with a different effective variance of the log normal size distribution (Madeleine et al., 2012; Navarro et al., 2014).

Heterogeneous production/loss rates will, via Equations 3 and 5, be proportional to aerosol number density, gas reactant number density, mean aerosol particle radius, temperature, and atmospheric density. In the two-moment scheme, however, aerosol number density is inversely proportional to the cube of partice radius (Madeleine et al., 2011). Heterogeneous production/loss rates should therefore be inversely proportional to particle radius.

2.4. Model Configuration

The MGCM was run at a spatial resolution of approximately $5° \times 5°$ gridboxes, and with 35 nonlinearly spaced topography-following vertical layers up to an altitude of approximately 90 km. The spatial (column) dust distribution was constrained by the dust maps for MY 34–36 of Montabone et al. (2015, 2020), though the vertical dust distribution was allowed to evolve freely through model advection. The model was run from $L_s = 150°$ of MY 34, corresponding to the beginning of the TGO science mission, until the end of MY 36. In the gas-phase chemistry only run, henceforth "Model-GP," HCl was initialized to 1 ppb by mass uniformly across all locations below approximately 50 km. All other chlorine species were initialized to 0. In the gas-phase and heterogeneous chemistry run, henceforth "Model-HET," HCl loss and production was controlled entirely by the heterogeneous processes in Equations 1 and 2.

2.5. HCl Observations

For this study we used publicly available HCl volume mixing ratio (VMR) retrieved profiles from TGO/ACS from $L_s = 163°$ of MY 34 to the end of MY 36. Full details of the observations, filtering, and solar occultation retrieval techniques can be found in Olsen et al. (2024a). Retrievals were reported on a 1 km vertical grid, and detections above 30 km with standard deviations >4 ppbv were rejected. The data set used here contains 494 HCl profiles, of which 467 (94.5%) occur during the dusty/perihelion season ($L_s \geq 180°$) and 27 (5.5%) occur during the clear/aphelion season ($L_s < 180°$) of their respective Mars Years. Measurements were made via solar occultation, and so retrieved profile values are for local dawn and dusk.

3. Results

Figures 1a and 1b displays the seasonal trends and latitudinal structure of both modeled and observed HCl. As noted in the existing literature, observed HCl abundances show a high degree of variation with both season and latitude. While there are some (5.5%) aphelion season detections, mostly <1 ppbv, the vast majority of observed HCl is present during the perihelion season. There is also a noticeable latitudinal bias during the perihelion season, with higher observed HCl in the southern hemisphere.

The Model-GP results in Figure 1a show minimal seasonal and latitudinal structure and do not correspond to observations. VMRs show slight (~20%) peaks at high northern and southern latitudes throughout the year (Rajendran et al., 2025). Elsewhere, including at tropical and mid-latitudes, the HCl distribution is highly uniform. There is no perihelion season increase or subsequent aphelion period decrease, and no hemispheric bias.

The Model-HET results in Figure 1b display seasonal and latitudinal behavior in line with observations. HCl VMRs are at their highest, >4 ppbv, during the MY 34 GDS ($L_s = 180$–$230°$), and show a bifurcated structure with greater latitudinal and temporal extent in the south than in the north. HCl values decay afterward, though remaining high at southern high latitudes and with a southern polar spike with the MY 34 B-storm ($L_s = 270°$) (following nomenclature of Kass et al. (2016)), before a brief spike with the MY 34 C-storm ($L_s = 320°$). Global HCl VMRs drop during the subsequent MY 35 aphelion season, though with high values (2–4 ppbv) around the southern seasonal cap edge and northern high/polar latitudes. The latter show a marked minimum between $L_s = 90$–$150°$. This may be due to increased HCl photolysis at northern high latitudes during the height of northern summer. However, ACS detection limits show no high aphelion abundances here. HCl is absent from the southern polar vortex in Model-HET, agreeing with observations.

The MY 35 perihelion season shows another HCl increase, in particular around the time of the MY 35 A-storm ($L_s = 220°$). HCl VMRs remain consistently higher in the southern hemisphere (2–4 ppbv) than the northern (1–2 ppbv), and show local maxima at times corresponding to the A,B,C regional dust storms. The perihelion season also shows strong exclusion of HCl from the northern polar vortex. This general structure of HCl distribution in a non-GDS year appears to be repeated in MY 36, though with varying intensities of the storm-linked HCl spikes. Notably, the MY 35 aphelion dust storm at $L_s = 45°$ did not appear to cause an enhancement in HCl in Model-HET or the observations. This may be due to the relative paucity of H atoms available for the heterogeneous dust reaction at northern latitudes during the aphelion season (Lefèvre & Krasnopolsky, 2017).

The observations in Figure 1c show nearly all retrieved profiles occurring during the perihelion season. The maximum values of HCl VMR in each profile occur at higher altitudes (30–50 km) earlier in the perihelion season of each year ($L_s = 180$–$270°$), before declining to lower altitudes (10–30 km) later ($L_s = 270$–$320°$). The result is an apparent descending HCl distribution. However, there does not seem to be a strong instantaneous correlation between HCl increases and dust storm activity, including from the GDS.

The Model-GP results in Figure 1d show a highly uniform HCl distribution with no apparent seasonal or altitude structure. The Model-HET results in Figure 1e show a sharp structure which matches observations. One notable point of agreement is the descending HCl distribution mentioned above, evident between $L_s = 230$–$320°$ of each MY. In Model-HET, this descending HCl structure is due to the gradual descent of atmospheric dust throughout the perihelion season. However, there are also points of disagreement. The Model-HET HCl shows maximum values during the early phase of the MY 34 GDS ($L_s = 190$–$240°$), while observations show enhanced values later after the GDS. This may be in part a function of difficult observing conditions under high dust loading, or evidence of a more indirect relationship between dust and HCl than in Model-HET. Observations also show

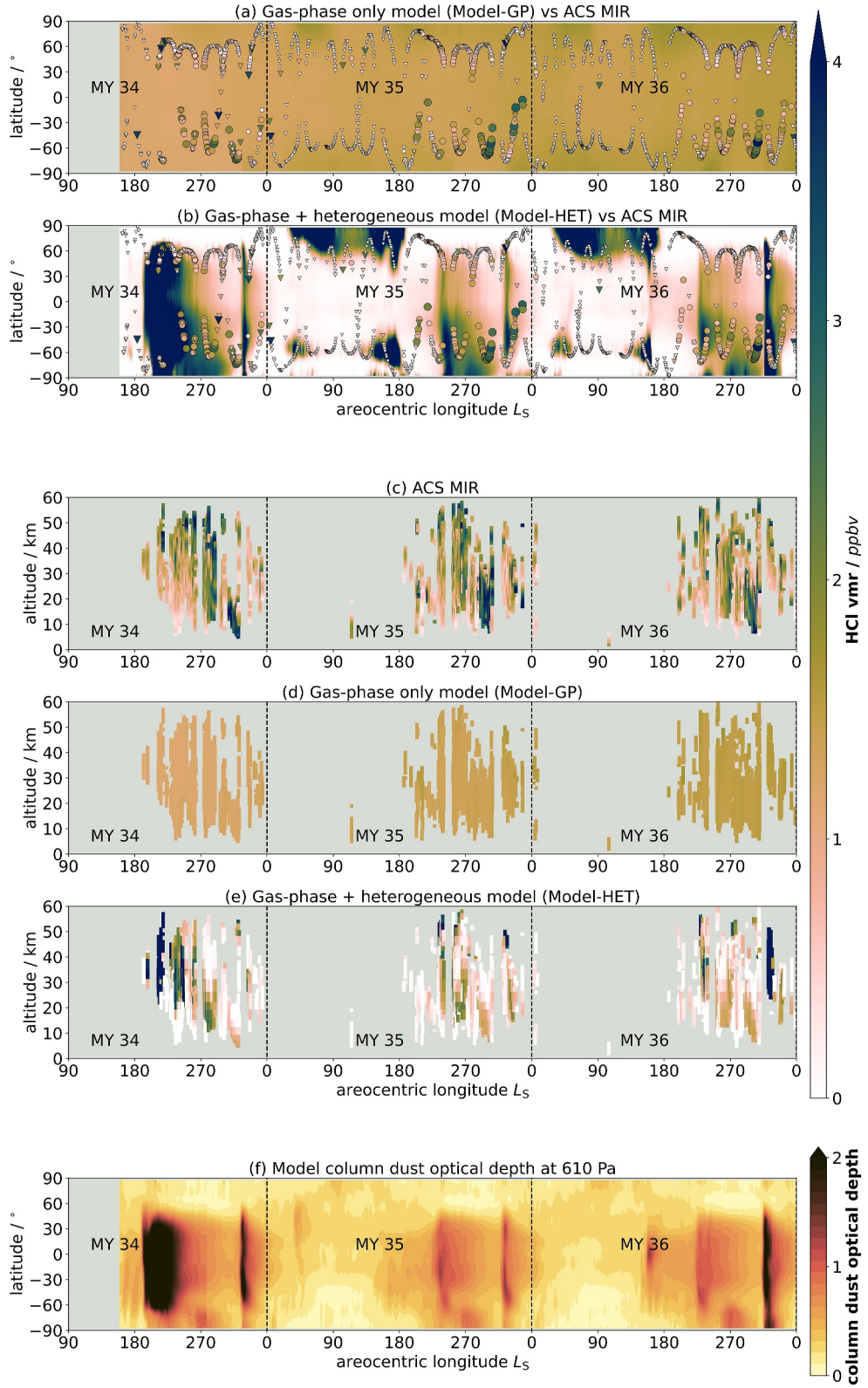
(a) Gas-phase only model (Model-GP) vs ACS MIR
(b) Gas-phase + heterogeneous model (Model-HET) vs ACS MIR
(c) ACS MIR
(d) Gas-phase only model (Model-GP)
(e) Gas-phase + heterogeneous model (Model-HET)
(f) Model column dust optical depth at 610 Pa
MY 34
MY 35
MY 36
latitude / °
altitude / km
areocentric longitude L_S
HCl vmr / ppbv
column dust optical depth

Figure 1.

apparently smoother variations in HCl abundances across individual profiles as compared to the sharper changes in Model-HET profiles.

Figure 2 shows a comparison of mean (a) and illustrative individual (b–d) HCl VMR profiles for the two model runs and the ACS observations, including the population standard deviation for the mean profiles. The mean observation profile has a VMR of around 1.5 ppbv between 10 and 40 km, rising both below 10 km and above 40 km to 2–3 ppbv. The high population standard deviation of 1–2 ppbv indicates significant vertical and temporal variability. This is in contrast to Model-GP, which shows a uniform mean profile with very low variation. The Model-HET mean structure shows increasing HCl VMR with altitude, from around 0.5 ppbv at 10 km to 2 ppbv at 50 km, with a high population standard deviation of over 3 ppbv above 30 km. While the mean profile of Model-GP shows reasonable agreement with observations between 10 and 40 km, it cannot capture the high spatial and temporal variability of the observed HCl.

In the three individual profiles in Figures 2b–2d the Model-GP results show a uniform HCl VMR with altitude while the observations and Model-HET show a high degree of vertical structure. The Model-HET results are able to approximate the general shape of the observed profiles, such as the peaks in VMR between 20 and 30 km in (b, c) and the HCl absence/minimum between 30 and 50 km in (d). Figures S1–S3 in Supporting Information S1 show similar comparisons as Figure 2, between the models and ACS water vapor (Olsen et al., 2024b), ACS water ice (Stcherbinine et al., 2020), and MCS dust (Kleinböhl et al., 2011) retrieved profiles. The water vapor distribution in Model-HET for profile (d) also shows the weakest agreement of the three profiles (Figure S1 in Supporting Information S1), and ACS observations indicate water ice presence not seen in the models. This suggests that a better model aerosol distribution would improve model HCl representation.

4. Discussion

Unlike Model-GP, Model-HET is able to reproduce key features of the observed atmospheric HCl distribution. One is the broad seasonal trend where HCl abundance increases in the perihelion season $L_s = 180°$, and decreases again after $L_s = 360°$ (Korablev et al., 2021; Olsen et al., 2021). In Model-HET, this seasonal variation is caused by the relative abundance of dust and water ice aerosols. Dust loading increases during the perihelion season, increasing the aerosol surface area for the source reaction Equation 1. This is evident in the correlation between HCl and large dust storms (Figure 1). During the colder and clearer aphelion season, lower atmosphere water ice clouds are more prevalent. This also applies to the northern polar vortex during the perihelion season.

Model-HET also reproduces broad features of the observed latitudinal and vertical HCl distribution. Observed HCl displays a latitudinal asymmetry during the perihelion season with greater abundances in the southern hemisphere (Aoki et al., 2021; Korablev et al., 2021; Olsen et al., 2021). Observed dust opacities during the perihelion season are also greater in the southern hemisphere (e.g., Montabone et al., 2015), including during regional dust storms (Kass et al., 2016), while water ice opacities are greater in the northern hemisphere particularly in the polar region (e.g., Haberle et al., 2019; Wolff et al., 2019). This aerosol latitudinal structure is reflected in the perihelion season Model-HET HCl abundances, which closely correlate with dust storm timings and structure (including hemispheric asymmetry) while being absent around the north polar hood (Figure 1b).

Model-HET captures some of the observed vertical variability and structure in HCl, unlike Model-GP. One point of agreement is the descending structure of HCl around the time of the MY 34 GDS, visible in Figures 1c and 1e. Given the absence of water ice, this shows that the dust source scheme provides a reasonable representation of HCl behavior under high dust loading. This descending structure is linked to the descending dust distribution after the initial and mature stages of the GDS (e.g., Bertrand et al., 2020), and similar dust height lowering during non-GDS perihelion seasons. This hints at similar causes in the observations. Altertnatively, this link could be indirect:

Figure 1. Observations and model fields with time against (a, b, f) latitude and (c, d, e) altitude. Panels (a, b) show maximum HCl volume mixing ratios for each profile from the MGCM between 10 and 40 km (filled contours), ACS MIR observations (circle markers), and ACS MIR detection limits (triangle markers). Marker size is proportional to HCl volume mixing ratio. Panels (c, d, e) show HCl volume mixing ratio observations and model values masked to fit closest observation times/locations; model HCl diurnal variability is minimal (see Figure S4 in Supporting Information S1). Panel (f) shows model column dust optical depth at 670 nm for the same periods. Model data in panels (a, b, f) has had a 5-sol running mean applied and is not masked to observation times/locations. Gray background indicates absence of model/observational data.

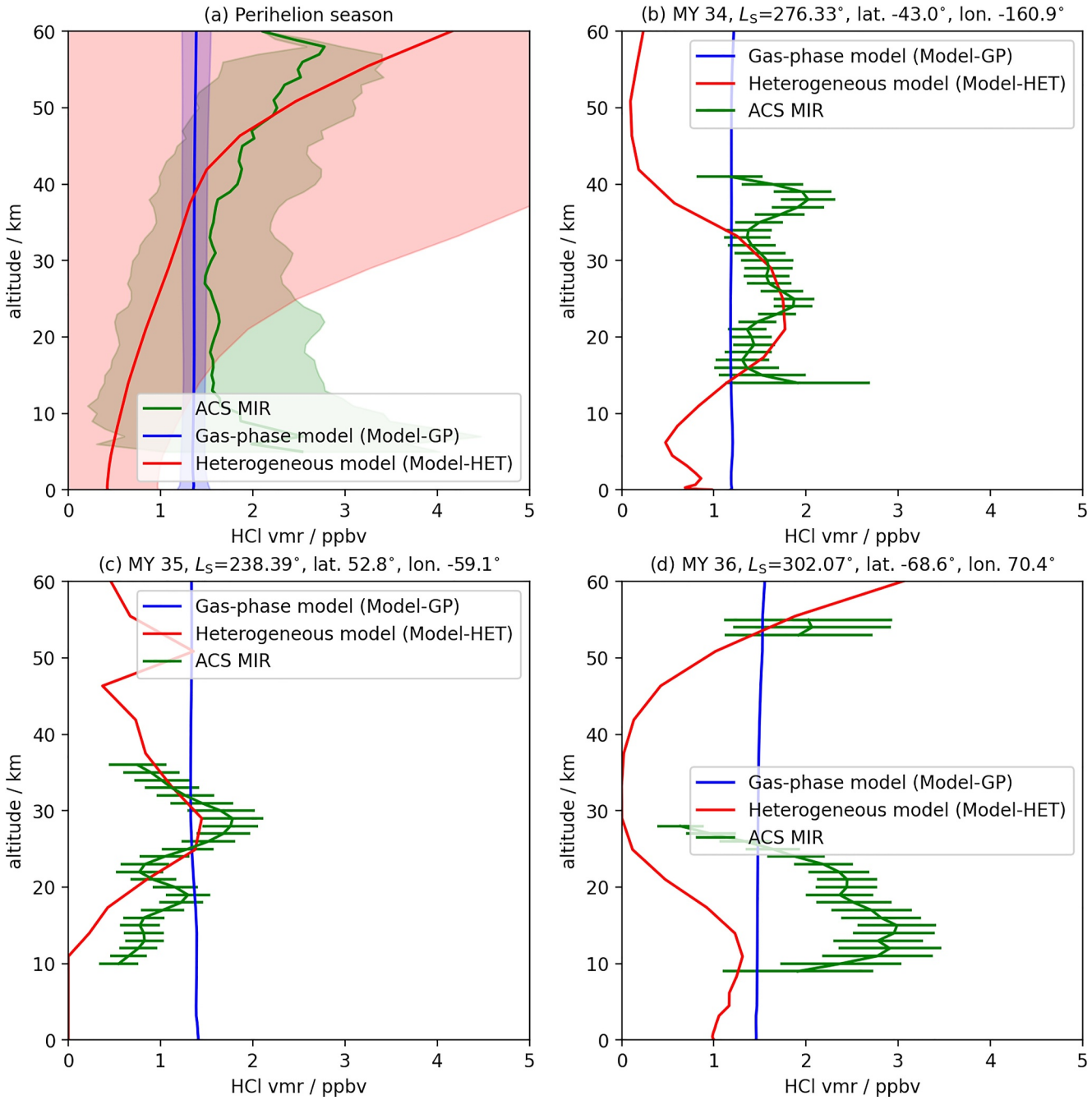

Figure 2. Comparison of atmospheric HCl profiles for ACS observations, gas-phase only model outputs, and heterogeneous model outputs. All model data is masked to best match the observation times and locations. Subplot (a) shows mean (solid lines) and population standard deviation (shaded area) for all observations/data within the perihelion seasons of MY 34–36. Subplots (b–d) show comparisons for individual observed profiles in MY 34–36, with error bars representing standard errors. Displayed L_s, latitude, and longitude values are for the observations. Values for Model-GP and Model-HET are within the closest 0.04° in L_s, and 2.5° in latitude/longitude.

for example, warmer temperatures from enhanced dust presence inhibiting water ice formation and/or sublimating HCl from existing water ice.

However, there are differences between the Model-HET results and observations. Two notable examples are high HCl abundances in Model-HET at high altitudes, Figure 2a, and at northern polar latitudes and the southern seasonal cap edge during aphelion season, Figure 1b. There are not unambiguous HCl detections above 60 km,

though this does not necessarily indicate its absence (Olsen et al., 2024a). In Model-HET these enhanced high-altitude abundances are linked to large number densities of submicron dust, which have been hypothesized (Montmessin et al., 2002) but not confirmed. The northern polar high HCl abundances in Model-HET seem more likely to be incorrect, given the predicted values of ≥4 ppbv compared to ACS detection limits between 0 and 1 ppbv. This disagreement is interesting as it results from the same heterogeneous mechanisms which provide a reasonable observational agreement during the perihelion season. The high vapor abundances (meaning available H via photolysis), moderate dust abundances, and ice absence which cause this enhancement in Model-HET are also visible in observational data (Smith, 2004). This model-observation disagreement implies that the current heterogeneous scheme is misrepresenting or missing some crucial process(es) that are either inhibiting HCl production or destroying it rapidly.

Another disagreement is the level of correlation between HCl abundance and dust opacity, particularly with large dust events. Model-HET naturally shows a close correlation between atmospheric dust loading and HCl abundance. This is evident in the HCl maximum VMR structure closely following GDS and regional dust storm dust timings (Montabone et al., 2015). The observed HCl, however, does not appear to show a strong correlation with dust opacity beyond its annual increase during the dusty season. Observations from ACS (Olsen et al., 2021) and NOMAD (Aoki et al., 2021) instead indicate strong vertical similarities between HCl and water vapor profiles. Olsen et al. (2024b) found weak correlation between HCl and dust and weak anticorrelation between HCl and water ice, but stronger correlation between HCl and water vapor. These analyses indicate that water vapor may have greater causal effects on HCl than aerosol, though the evidence of ice-holes provides a compelling case for a water ice and HCl causal relation (Luginin et al., 2024).

Other evidence suggests a more direct role for dust in HCl creation. HCl isotopologue measurements suggest chlorine bearing dust grains are linked to HCl formation (Trokhimovskiy et al., 2021), and the established presence of surface perchlorates implies chlorine species adsorption onto martian soil. 1D modeling work suggests that a wider range of reactions than presented here could be the impetus for future GCM work. Krasnopolsky (2022) included reactions for mineral dust as a sink for Cl and a source for ClO, and water ice as a sink for HCl/HOCl and source for Cl_2. They were able to replicate lower atmosphere HCl profiles and seasonal variation in a 1D model, with HCl VMR increasing above the ACS cutoff. Taysum et al. (2024) modeled dust as a Cl source via UV photolysis, together with water ice and dust as sinks, and were able to reproduce ACS profiles though with HCl VMR decreasing at the ACS cutoff (*contra* Krasnopolsky (2022)).

Our results strongly suggest that heterogeneous processes play a key role in explaining the observed global distribution of HCl and its seasonal, latitudinal, and vertical structure. In the context of previous observational and 1D modeling work, it is likely that water ice has a direct causal relationship to HCl via heterogeneous processes. The role of dust is more debatable; the relationships between dust, vapor, ice, and the seasonal cycle make it difficult to ascertain whether atmospheric dust has solely an indirect relationship with HCl via its links to vapor and ice, or also a direct causal relationship via heterogeneous processes. Another possibility is temperature dependence of heterogeneous reactions; a strong temperature dependence in reaction probabilities could help to account for model-observation discrepancies during aphelion and at high altitudes. Lastly, it appears that particle size is important in determining heterogeneous impacts; for example, smaller dust particles at higher altitudes, with greater surface area per unit mass available for reactions, seem to have an outsized effect and contribute to higher HCl abundances, both directly and via lofting. The role of particle sizes (in both source and sink reactions) requires further investigation.

Future work will aim to improve atmospheric aerosol and water vapor representation via data assimilation, combining GCM with observations from various spacecraft. It will also explore further heterogeneous chlorine reactions and in particular the role of dust as a chlorine sink via adsorption and water ice as a chlorine source via release of previously adsorbed chlorine. The adsorption-sublimation scheme of Brown et al. (2022) for OH and water ice offers a way forward for these investigations. In addition, future work would be well-served by further laboratory experiments to measure and constrain heterogeneous reaction rates, uptake coefficients, and chemical lifetimes for gases on chlorine-containing minerals and water ice under martian conditions (temperatures, pressures, atmospheric composition, incident radiation), including in suspended aerosol form to evaluate any particle size dependencies.

5. Conclusions

We have incorporated for the first time heterogeneous chlorine chemistry into a Mars global climate model, representing atmospheric mineral dust as an HCl source and water ice as an HCl sink.

1. The inclusion of heterogeneous chemistry shows significant improvements in the HCl distribution relative to ACS HCl observations, as compared to gas-phase only modeling.
2. The heterogeneous model is able to reproduce key observed global HCl features such as overall abundances; seasonal enhancement and reduction; the observed latitudinal asymmetry, represented as a greater HCl presence in the southern hemisphere in the model; lowering of the HCl profile with altitude following large dust events; and altitudinal variation.
3. However, there are disagreements. The heterogeneous model displays a close correlation between dust and HCl abundance not necessarily apparent in the observations. The model also predicts high HCl abundances at northern high latitudes during aphelion season not currently seen in ACS retrievals.
4. Accurate representation of atmospheric aerosols (dust, water ice) and key species (water vapor) is important for determining HCl heterogeneous behavior.
5. Our results suggest that heterogeneous chlorine chemistry is key for explaining the observed distribution of atmospheric HCl on Mars, but further work is required to adequately represent and understand the exact heterogeneous reactions involved.

Data Availability Statement

HCl observations are publicly available from Olsen et al. (2024a). Model data is publicly available on ORDO (Streeter, Rajendran, et al., 2024).

Acknowledgments
PS, KR, and SRL acknowledge funding from the UK Space Agency (UKSA) under grant ST/W002949/1. MRP acknowledges UKSA funding through Grants ST/V002295/1, ST/Y005929/1, ST/X006549/1, ST/Y006054/1, and ST/Y000234/1. KO acknowledges funding from UKSA under grants ST/T002069/1 and ST/Y000196/1. AT and OK acknowledge funding from Roscosmos and the Ministry of Science and Education in Russia. PS thanks Aurélien Stcherbinine for ACS water ice retrievals. The Scientific Colour Maps suite was used for plots (Crameri, 2020). We would also like to thank two anonymous reviewers for their helpful comments.

References

Aoki, S., Daerden, F., Viscardy, S., Thomas, I. R., Erwin, J. T., Robert, S., et al. (2021). Annual appearance of hydrogen chloride on Mars and a striking similarity with the water vapor vertical distribution observed by TGO/NOMAD. *Geophysical Research Letters*, *48*(11), e2021GL092506. https://doi.org/10.1029/2021GL092506

Atkinson, R., Baulch, D. L., Cox, R. A., Crowley, J. N., Hampson, R. F., Hynes, R. G., et al. (2007). Evaluated kinetic and photochemical data for atmospheric chemistry: Volume III—Gas phase reactions of inorganic halogens. *Atmospheric Chemistry and Physics*, *7*(4), 981–1191. https://doi.org/10.5194/acp-7-981-2007

Barnes, R., Sinha, A., & Michelsen, H. (1998). Assessing the contribution of the lowest triplet state to the near-UV absorption spectrum of HOCl. *Journal of Physical Chemistry A*, *102*(45), 8855–8859. https://doi.org/10.1021/jp9835869

Baulch, D. L., Bowman, C. T., Cobos, C. J., Cox, R. A., Just, T., Kerr, J. A., et al. (2005). Evaluated kinetic data for combustion modeling: Supplement II. *Journal of Physical and Chemical Reference Data*, *34*(3), 757–1397. https://doi.org/10.1063/1.1748524

Bertrand, T., Wilson, R. J., Kahre, M. A., Urata, R., & Kling, A. (2020). Simulation of the 2018 global dust storm on Mars using the NASA Ames Mars GCM: A multitracer approach. *Journal of Geophysical Research: Planets*, *125*(7), e2019JE006122. https://doi.org/10.1029/2019JE006122

Brasseur, G., & Solomon, S. (1986). *Aeronomy of the middle atmosphere: Chemistry and physics of the stratosphere and mesosphere* (2nd ed.). D. Reidel.

Brown, M. a. J., Patel, M. R., Lewis, S. R., Holmes, J. A., Sellers, G. J., Streeter, P. M., et al. (2022). Impacts of heterogeneous chemistry on vertical profiles of Martian Ozone. *Journal of Geophysical Research: Planets*, *127*(11), e2022JE007346. https://doi.org/10.1029/2022JE007346

Burkholder, J. B., Sander, S. P., Abbatt, J., Barker, J. R., Cappa, C., Crounse, J. D., et al. (2019). *Chemical kinetics and photochemical data for use in atmospheric studies, evaluation no. 19 (JPL Publication 19-5)*. Jet Propulsion Laboratory, Pasadena. Retrieved from http://jpldataeval.jpl.nasa.gov/

Campbell, I. M., & Gray, C. N. (1973). Rate constants for O(3P) recombination and association with N(4S). *Chemical Physics Letters*, *18*(4), 607–609. https://doi.org/10.1016/0009-2614(73)80479-8

Catling, D. C., Claire, M. W., Zahnle, K. J., Quinn, R. C., Clark, B. C., Hecht, M. H., & Kounaves, S. (2010). Atmospheric origins of perchlorate on Mars and in the Atacama. *Journal of Geophysical Research*, *115*(E1). https://doi.org/10.1029/2009JE003425

Chapman, R., Lewis, S., Balme, M., & Steele, L. (2017). Diurnal variation in Martian dust devil activity. *Icarus*, *292*, 154–167. https://doi.org/10.1016/j.icarus.2017.01.003

Cheng, B.-M., Chew, E., Liu, C.-P., Bahou, M., Lee, Y.-P., Yung, Y., & Gerstell, M. (1999). Photo-induced fractionation of water isotopomers in the Martian atmosphere. *Geophysical Research Letters*, *26*(24), 3657–3660. https://doi.org/10.1029/1999gl008367

Clark, J. V., Sutter, B., McAdam, A. C., Rampe, E. B., Archer, P. D., Ming, D. W., et al. (2020). High-temperature HCl evolutions from mixtures of perchlorates and chlorides with water-bearing phases: Implications for the SAM instrument in Gale Crater, Mars. *Journal of Geophysical Research: Planets*, *125*(2), e2019JE006173. https://doi.org/10.1029/2019JE006173

Crameri, F. (2020). *Scientific colour maps*. Zenodo. https://doi.org/10.5281/zenodo.4153113

Forget, F., Hourdin, F., Fournier, R., Hourdin, C., Talagrand, O., Collins, M., et al. (1999). Improved general circulation models of the Martian atmosphere from the surface to above 80 km. *Journal of Geophysical Research*, *104*(E10), 24155–24175. https://doi.org/10.1029/1999JE001025

George, I. J., & Abbatt, J. P. D. (2010). Heterogeneous oxidation of atmospheric aerosol particles by gas-phase radicals. *Nature Chemistry*, *2*(9), 713–722. https://doi.org/10.1038/nchem.806

Haberle, R. M., Kahre, M. A., Barnes, J. R., Hollingsworth, J. L., & Wolff, M. J. (2019). MARCI observations of a wavenumber-2 large-scale feature in the north polar hood of Mars: Interpretation with the NASA/Ames Legacy Global Climate Model. *Icarus*, *335*, 113367. https://doi.org/10.1016/j.icarus.2019.07.001

Hartogh, P., Jarchow, C., Lellouch, E., Val-Borro, M. d., Rengel, M., Moreno, R., et al. (2010). Herschel/HIFI observations of Mars: First detection of O_2 at submillimetre wavelengths and upper limits on HCl and H2O2. *Astronomy & Astrophysics*, *521*, L49. https://doi.org/10.1051/0004-6361/201015160

Holmes, J. A., Lewis, S. R., Patel, M. R., Chaffin, M. S., Cangi, E. M., Deighan, J., et al. (2021). Enhanced water loss from the Martian atmosphere during a regional-scale dust storm and implications for long-term water loss. *Earth and Planetary Science Letters*, *571*, 117109. https://doi.org/10.1016/j.epsl.2021.117109

Holmes, J. A., Lewis, S. R., Patel, M. R., & Lefèvre, F. (2018). A reanalysis of ozone on Mars from assimilation of SPICAM observations. *Icarus*, *302*, 308–318. https://doi.org/10.1016/j.icarus.2017.11.026

Hoskins, B. J., & Simmons, A. J. (1975). A multi-layer spectral model and the semi-implicit method. *Quarterly Journal of the Royal Meteorological Society*, *101*(429), 637–655. https://doi.org/10.1002/qj.49710142918

Jacob, D. J. (2000). Heterogeneous chemistry and tropospheric ozone. *Atmospheric Environment*, *34*(12), 2131–2159. https://doi.org/10.1016/S1352-2310(99)00462-8

Kass, D. M., Kleinböhl, A., McCleese, D. J., Schofield, J. T., & Smith, M. D. (2016). Interannual similarity in the Martian atmosphere during the dust storm season. *Geophysical Research Letters*, *43*(12), https://doi.org/10.1002/2016GL068978

Kleinböhl, A., Schofield, J. T., Abdou, W. A., Irwin, P. G. J., & de Kok, R. J. (2011). A single-scattering approximation for infrared radiative transfer in limb geometry in the Martian atmosphere. *Journal of Quantitative Spectroscopy and Radiative Transfer*, *112*(10), 1568–1580. https://doi.org/10.1016/j.jqsrt.2011.03.006

Korablev, O., Olsen, K. S., Trokhimovskiy, A., Lefèvre, F., Montmessin, F., Fedorova, A. A., et al. (2021). Transient HCl in the atmosphere of Mars. *Science Advances*, *7*(7), eabe4386. https://doi.org/10.1126/sciadv.abe4386

Krasnopolsky, V. A. (2022). Photochemistry of HCl in the Martian atmosphere. *Icarus*, *374*, 114807. https://doi.org/10.1016/j.icarus.2021.114807

Lefèvre, F., & Krasnopolsky, V. (2017). Atmospheric photochemistry. In F. Forget, M. D. Smith, R. T. Clancy, R. W. Zurek, & R. M. Haberle (Eds.), *The atmosphere and climate of Mars* (pp. 405–432). Cambridge University Press. https://doi.org/10.1017/9781139060172.013

Lefèvre, F., Lebonnois, S., Montmessin, F., & Forget, F. (2004). Three-dimensional modeling of ozone on Mars. *Journal of Geophysical Research*, *109*(E7). https://doi.org/10.1029/2004JE002268

Lewis, B., & Carver, J. (1983). Temperature dependence of the carbon dioxide photoabsorption cross section between 1200 and 1970 Å. *Journal of Quantitative Spectroscopy and Radiative Transfer*, *30*(4), 297–309. https://doi.org/10.1016/0022-4073(83)90027-4

Lewis, S. R., Mulholland, D. P., Read, P. L., Montabone, L., Wilson, R. J., & Smith, M. D. (2016). The solsticial pause on Mars: 1. A planetary wave reanalysis. *Icarus*, *264*, 456–464. https://doi.org/10.1016/j.icarus.2015.08.039

Lewis, S. R., & Read, P. L. (2003). Equatorial jets in the dusty Martian atmosphere. *Journal of Geophysical Research*, *108*(E4). https://doi.org/10.1029/2002JE001933

Liuzzi, G., Villanueva, G. L., Viscardy, S., Mège, D., Crismani, M. M. J., Aoki, S., et al. (2021). Probing the atmospheric Cl isotopic ratio on Mars: Implications for planetary evolution and atmospheric chemistry. *Geophysical Research Letters*, *48*(9), e2021GL092650. https://doi.org/10.1029/2021GL092650

Luginin, M., Trokhimovskiy, A., Taysum, B., Fedorova, A. A., Korablev, O., Olsen, K. S., et al. (2024). Evidence of rapid hydrogen chloride uptake on water ice in the atmosphere of Mars. *Icarus*, *411*, 115960. https://doi.org/10.1016/j.icarus.2024.115960

Madeleine, J.-B., Forget, F., Millour, E., Montabone, L., & Wolff, M. J. (2011). Revisiting the radiative impact of dust on Mars using the LMD Global Climate Model. *Journal of Geophysical Research*, *116*(E11), E11010. https://doi.org/10.1029/2011JE003855

Madeleine, J.-B., Forget, F., Millour, E., Navarro, T., & Spiga, A. (2012). The influence of radiatively active water ice clouds on the Martian climate. *Geophysical Research Letters*, *39*(23). https://doi.org/10.1029/2012GL053564

Minschwaner, K., Anderson, G., Hall, L., & Yoshino, K. (1992). Polynomial coefficients for calculating O_2 Schumann-Runge cross sections at 0.5 cm- 1 resolution. *Journal of Geophysical Research*, *97*(D9), 10103–10108. https://doi.org/10.1029/92jd00661

Montabone, L., Forget, F., Millour, E., Wilson, R. J., Lewis, S. R., Cantor, B., et al. (2015). Eight-year climatology of dust optical depth on Mars. *Icarus*, *251*, 65–95. https://doi.org/10.1016/j.icarus.2014.12.034

Montabone, L., Spiga, A., Kass, D. M., Kleinböhl, A., Forget, F., & Millour, E. (2020). Martian Year 34 column dust climatology from mars climate sounder observations: Reconstructed maps and model simulations. *Journal of Geophysical Research: Planets*, *125*(8), e2019JE006111. https://doi.org/10.1029/2019JE006111

Montmessin, F., Rannou, P., & Cabane, M. (2002). New insights into Martian dust distribution and water-ice cloud microphysics. *Journal of Geophysical Research*, *107*(E6), 4-1–4-14. https://doi.org/10.1029/2001JE001520

Mulholland, D. P., Spiga, A., Listowski, C., & Read, P. L. (2015). An assessment of the impact of local processes on dust lifting in Martian climate models. *Icarus*, *252*, 212–227. https://doi.org/10.1016/j.icarus.2015.01.017

Navarro, T., Madeleine, J.-B., Forget, F., Spiga, A., Millour, E., Montmessin, F., & Määttänen, A. (2014). Global climate modeling of the Martian water cycle with improved microphysics and radiatively active water ice clouds. *Journal of Geophysical Research: Planets*, *119*(7), 1479–1495. https://doi.org/10.1002/2013JE004550

Newman, C. E., Lewis, S. R., Read, P. L., & Forget, F. (2002). Modeling the Martian dust cycle, 1. Representations of dust transport processes. *Journal of Geophysical Research*, *107*(E12), 5123. https://doi.org/10.1029/2002JE001910

Olsen, K. S., Fedorova, A. A., Kass, D. M., Kleinböhl, A., Trokhimovskiy, A., Korablev, O. I., et al. (2024a). Relationships between HCl, H_2O, aerosols, and temperature in the Martian atmosphere: 1. Climatological outlook. *Journal of Geophysical Research: Planets*, *129*(8), e2024JE008350. https://doi.org/10.1029/2024JE008350

Olsen, K. S., Fedorova, A. A., Kass, D. M., Kleinböhl, A., Trokhimovskiy, A., Korablev, O. I., et al. (2024b). Relationships between HCl, H_2O, aerosols, and temperature in the Martian atmosphere: 2. Quantitative correlations. *Journal of Geophysical Research: Planets*, *129*(8), e2024JE008351. https://doi.org/10.1029/2024JE008351

Olsen, K. S., Trokhimovskiy, A., Montabone, L., Fedorova, A. A., Luginin, M., Lefèvre, F., et al. (2021). Seasonal reappearance of HCl in the atmosphere of Mars during the Mars year 35 dusty season. *Astronomy & Astrophysics*, *647*, A161. https://doi.org/10.1051/0004-6361/202140329

Papanastasiou, D., Papadimitriou, V., Fahey, D., & Burkholder, J. (2009). UV absorption spectrum of the ClO dimer (Cl2O2) between 200 and 420 nm. *Journal of Physical Chemistry A*, *113*(49), 13711–13726. https://doi.org/10.1021/jp9065345

Parkinson, W., Rufus, J., & Yoshino, K. (2003). Absolute absorption cross section measurements of CO_2 in the wavelength region 163–200 nm and the temperature dependence. *Chemical Physics*, *290*(2–3), 251–256. https://doi.org/10.1016/s0301-0104(03)00146-0

Rajendran, K., Lewis, S. R., Holmes, J. A., Streeter, P. M., Fedorova, A. A., & Patel, M. R. (2021). Enhanced super-rotation before and during the 2018 Martian global dust storm. *Geophysical Research Letters*, *48*(16), e2021GL094634. https://doi.org/10.1029/2021GL094634

Rajendran, K., Streeter, P. M., Lewis, S. R., Duffy, M. K. D., Holmes, J. A., Olsen, K. S., et al. (2025). Global transport of chlorine species in the Martian atmosphere and the resulting surface distribution of perchlorates. *Journal of Geophysical Research: Planets*. https://doi.org/10.1029/2024JE008537

Sander, S., Abbatt, J., Barker, J., Burkholder, J., Friedl, R., Golden, D., et al. (2011). Chemical kinetics and photochemical data for use in atmospheric studies, Evaluation no. 17 (Tech. Rep. No. 10-6).

Sander, S., Friedl, R., Golden, D., Kurylo, M., Huie, R., Orkin, V., et al. (2003). Chemical kinetics and photochemical data for use in atmospheric studies. Evaluation no. 14 (Tech. Rep. No. 02-25).

Sander, S., Friedl, R., Golden, D., Kurylo, M., Moortgat, G., Wine, P., et al. (2006). Chemical kinetics and photochemical data for use in atmospheric studies, Evaluation no. 15 (Tech. Rep. No. 06-2).

Schergers, M., & Welge, K. (1968). Absorption coefficient of H202 and N2H4 between 1200 and 2000 Å. *Zeitschrift für Naturforschung A*, (10), 1508.

Simonaitis, R., & Heicklen, J. (1975). Perchloric acid: A possible sink for stratospheric chlorine. *Planetary and Space Science*, *23*(11), 1567–1569. https://doi.org/10.1016/0032-0633(75)90010-0

Simpson, W. R., Brown, S. S., Saiz-Lopez, A., Thornton, J. A., & von Glasow, R. (2015). Tropospheric halogen chemistry: Sources, cycling, and impacts. *Chemical Reviews*, *115*(10), 4035–4062. https://doi.org/10.1021/cr5006638

Smith, M. D. (2004). Interannual variability in TES atmospheric observations of Mars during 1999–2003. *Icarus*, *167*(1), 148–165. https://doi.org/10.1016/j.icarus.2003.09.010

Stcherbinine, A., Vincendon, M., Montmessin, F., Wolff, M. J., Korablev, O., Fedorova, A., et al. (2020). Martian water ice clouds during the 2018 global dust storm as observed by the ACS-MIR channel onboard the trace gas orbiter. *Journal of Geophysical Research: Planets*, *125*(3), e2019JE006300. https://doi.org/10.1029/2019JE006300

Steele, L. J., Lewis, S. R., & Patel, M. R. (2014). The radiative impact of water ice clouds from a reanalysis of Mars Climate Sounder data. *Geophysical Research Letters*, *41*(13), 4471–4478. https://doi.org/10.1002/2014GL060235

Steele, L. J., Lewis, S. R., Patel, M. R., Montmessin, F., Forget, F., & Smith, M. D. (2014). The seasonal cycle of water vapour on Mars from assimilation of thermal emission spectrometer data. *Icarus*, *237*, 97–115. https://doi.org/10.1016/j.icarus.2014.04.017

Streeter, P. M., Lewis, S. R., Patel, M. R., Holmes, J. A., Fedorova, A. A., Kass, D. M., & Kleinböhl, A. (2021). Asymmetric impacts on Mars' polar vortices from an equinoctial global dust storm. *Journal of Geophysical Research: Planets*, *126*(5), e2020JE006774. https://doi.org/10.1029/2020JE006774

Streeter, P. M., Lewis, S. R., Patel, M. R., Holmes, J. A., & Rajendran, K. (2024). An eight-year climatology of the Martian northern polar vortex. *Icarus*, *409*, 115864. https://doi.org/10.1016/j.icarus.2023.115864

Streeter, P. M., Rajendran, K., Lewis, S. R., & Patel, M. R. (2024). Global distribution and seasonality of Martian atmospheric HCl explained through heterogeneous chemistry - Dataset [Dataset]. *The Open University*. https://doi.org/10.21954/ou.rd.26089588.v1

Taysum, B. M., Palmer, P. I., Olsen, K., Luginin, M., Ignatiev, N., Trokhimovskiy, A., et al. (2024). Observed seasonal changes in Martian hydrogen chloride explained by heterogeneous chemistry. *Astronomy & Astrophysics*, *687*, A191. https://doi.org/10.1051/0004-6361/202449546

Trokhimovskiy, A., Fedorova, A. A., Olsen, K. S., Alday, J., Korablev, O., Montmessin, F., et al. (2021). Isotopes of chlorine from HCl in the Martian atmosphere. *Astronomy & Astrophysics*, *651*, A32. https://doi.org/10.1051/0004-6361/202140916

Trolier, M., Mauldin, R., & Ravishankara, A. (1990). Rate coefficient for the termolecular channel of the self-reaction of chlorine monoxide. *Journal of Physical Chemistry*, *94*(12), 4896–4907. https://doi.org/10.1021/j100375a027

Villanueva, G. L., Mumma, M. J., Novak, R. E., Radeva, Y. L., Käufl, H. U., Smette, A., et al. (2013). A sensitive search for organics (CH4, CH3OH, H2CO, C2H6, C2H2, C2H4), hydroperoxyl (HO2), nitrogen compounds (N2O, NH3, HCN) and chlorine species (HCl, CH3Cl) on Mars using ground-based high-resolution infrared spectroscopy. *Icarus*, *223*(1), 11–27. https://doi.org/10.1016/j.icarus.2012.11.013

Wahner, A., Tyndall, G., & Ravishankara, A. (1987). Absorption cross sections for symmetric chlorine dioxide as a function of temperature in the wavelength range 240-480nm. *Journal of Physical Chemistry*, *91*(11), 2734–2738. https://doi.org/10.1021/j100295a018

Wolff, M. J., Clancy, R. T., Kahre, M. A., Haberle, R. M., Forget, F., Cantor, B. A., & Malin, M. C. (2019). Mapping water ice clouds on Mars with MRO/MARCI. *Icarus*, *332*, 24–49. https://doi.org/10.1016/j.icarus.2019.05.041

Xu, Z. F., & Lin, M. C. (2003). Ab initio studies of ClOx reactions. IX. Combination and disproportionation reactions of ClO and s-ClO3 radicals. *The Journal of Chemical Physics*, *119*(17), 8897–8904. https://doi.org/10.1063/1.1613632

Yoshino, K., Cheung, A.-C., Esmond, J., Parkinson, W., Freeman, D., Guberman, S., et al. (1988). Improved absorption cross-sections of oxygen in the wavelength region 205–240 nm of the Herzberg continuum. *Planetary and Space Science*, *36*(12), 1469–1475. https://doi.org/10.1016/0032-0633(88)90012-8

Yoshino, K., Esmond, J., Parkinson, W., Ito, K., & Matsui, T. (1996). Absorption cross section measurements of water vapor in the wavelength region 120 to 188 nm. *Chemical Physics*, *211*(1–3), 387–391. https://doi.org/10.1016/0301-0104(96)00210-8

Yoshino, K., Esmond, J., Sun, Y., Parkinson, W., Ito, K., & Matsui, T. (1996). Absorption cross section measurements of carbon dioxide in the wavelength region 118.7–175.5 nm and the temperature dependence. *Journal of Quantitative Spectroscopy and Radiative Transfer*, *55*(1), 53–60. https://doi.org/10.1016/0022-4073(95)00135-2

Zhu, R. S., & Lin, M. C. (2004). Ab Initio studies of ClOx reactions: Prediction of the rate constants of ClO+NO for the forward and reverse processes. *ChemPhysChem*, *5*(12), 1864–1870. https://doi.org/10.1002/cphc.200400305